

The hereditary of the microstructure and texture in non-oriented electrical steels

TIE YE*, ZHI-WEN LU, ZHI-GUO ZHONG, CHUN-HUA MA

New Materials Engineering Technology Center, Nan yang Normal University, Nanyang 473061, Henan, China

Magnetic properties of non-oriented electrical steel are controlled to the greatest degree by the final texture and the final average grain size. In this paper, we study the hereditary of the microstructure and crystallographic texture in non-oriented electrical steel. Through the hereditary was investigated, we found: The bigger of the value of the proportion of the texture for $\{100\} + \text{Goss}\} / \{111\}$ is better magnetic properties, which reflect the texture hereditary. Gauss texture promotes magnetic induction increases. We can control the organization to control the texture pattern and control magnetic properties finally.

(Received June 9, 2014; accepted June 9, 2016)

Keywords: Hereditary, Microstructure, Texture, Magnetic properties

1. Introduction

The non-oriented electrical steel is a magnetically soft material, which is widely used in electric generators and motors. In general world production of transformer steels, the non-oriented steel occupies about 70%. Approximately half the electrical energy produced in the world is used in motor; therefore, the necessity of reducing the energy loss in these steels is economically substantiated and stimulates studies on the improvement of the quality of materials [1-6].

Magnetic properties of non-oriented electrical steel are controlled to the greatest degree by two characteristics of structure, namely, in the final texture and by the final average grain size. It is desirable to develop a strong $\{hk0\} \langle 001 \rangle$ texture component and to suppress the $\{111\} \langle uvw \rangle$ component. These metallurgical factors change with the chemical composition as well as processing conditions. In the production process, the second phase particles will affect the grain size and distribution of recrystallization texture. Controlling precipitation behavior of is important for obtaining proper microstructures and excellent magnetic properties of non-oriented electrical steels [7-13].

In this paper, we undertook an attempt to study the hereditary of the microstructure and crystallographic texture in non-oriented electrical steel i.e., evolution of microstructure and crystallographic texture in electrical steel in hot rolling, normalizing and annealing production process and the effect of the second phase [14-17] MnS on the organization and texture of the hereditary in non-oriented electrical steels. Through the hereditary was investigated, we hope to improve the magnetic properties of non-oriented electrical steel.

2. Experimented

The chemical composition (mass percent) of the tested steels is given in Table 1. Hot rolling slabs (Steel A and B) at 1123°C were hot rolled to 2.3mm steel coils, normalized at 970°C, cold rolled to 0.35mm steel coil with Sendzimir mill and finally annealed at 950°C in continuous annealing furnace. The microstructures of hot-band specimens, normalization specimens and annealing specimens were observed by optical microscopy. Texture of all the specimens was measured with Mo radiation using a Siemens D-5000 X-ray diffract meter. Three incomplete pole figures were measured and the orientation distribution function (ODF) was calculated by TexTools, a commercial software for texture analysis. Method of measurement of magnetic properties of electrical steel and strip by means of Epstein frame is according to the national standard of GB/T3655-2008 determination: As the magnetic properties, magnetic induction at 5000A/m (B_{50}) and the core loss at induction of 1.5T and 50Hz ($P_{15/50}$) were measured. The measurements were done in both rolling and transverse directions and the data were averaged to provide a representative value.

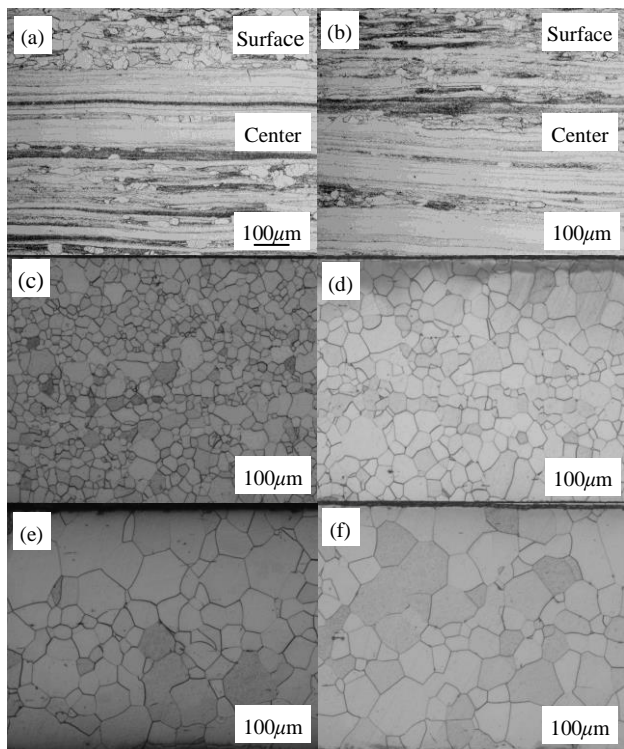
Table 1. Chemical composition of the tested steels (wt%)

No.	C	Si	Mn	P	S
A	0.0024	2.515	0.210	0.015	0.0037
B	0.0025	2.518	0.215	0.014	0.0019

3. Result and discussion

3.1 Microstructure hereditary

The microstructure of the hot band shows inhomogeneous character through the thickness, shown in Fig. 1a and Fig. 1b. Recrystallization equiaxed grains are found in the surface area but elongated recovered grains exist in the center. One reason for the difference in the microstructure between the surface and center areas is that the temperature gradient occurs through the thickness. Deformation at lower temperatures increases the amount of stored energy. This is because there is less thermal energy to assist in the release of energy and reduce the interaction between defects during deformation. During hot rolling, the stored energy at the surface area is on average high enough, due to its lower temperature, for dynamic recrystallization to take place. The stored energy in the center is not high enough for complete dynamic recrystallization due to its higher temperature during deformation. Higher temperatures allow more recovery to occur before the initiation of recrystallization. The structure with rolling ferrite and ferrite is easy to produce corrugated surface defects after cold rolling and annealing process; The microstructure of the normalization coil shows homogeneous character and grain size is relatively uniform shown in Fig. 1c and Fig. 1d; The microstructure of the annealing coil shows homogeneous character and grain size is even and larger than that of the normalization coil shown in Fig. 1e and Fig. 1f.



(a), (b) hot-band; (c), (d) normalization coil; (e)(f) annealing coil

Fig. 1. Optical microstructure of the specimen

The amount of recrystallization grain at the surface in Fig. 1a is more than that in Fig. 1b. The test coil A's S content is higher than that of in the test coil B.S and Mn is easy to form second-phase particles MnS (shown in, Fig. 2). The typical MnS second-phase particles exist in hot rolled coil, normalization coil and annealing coil and are little dimensional change in all process). The number of particles and the content of S are proportional to. These large and hard and wide spacing between the particles, due to deformation of particles near appear more inhomogeneous deformation area, these areas have large microscopically orientation difference, can promote nucleation (Particle Stimulated Nucleation) thus forming a Fig. 1 a in the surface more recrystallization grain size than that of in Fig. 1 b.

In the normalization, the test coil A formed more recrystallization grain and the energy storage was released, causing constant of nucleation rate decreased, so under the same conditions (the same time normalization), normalization grain of the test coil A in Fig. 1 c in the crystal grain is slightly less than that of in the Fig. 1 d.

The grain size in Fig. 1e is slightly less than that in the Fig. 1 f because the amount of the test coil A's MnS is much more than that of the test coil B, while the second phase particles it produces drag effect on migration of a grain boundary, obstructs the growth of grains. The elements of second phase are the limited solid solution in grain. When the grain boundaries migrate and meet a second phase particle, the boundary was distorted into arch and the interfacial area increases and at that time, the he pinning force produced by the second phase particles and the driving force of grain boundary curvature are equal. So the grain size in Fig. 1e is slightly less than that in the Fig. 1 f.

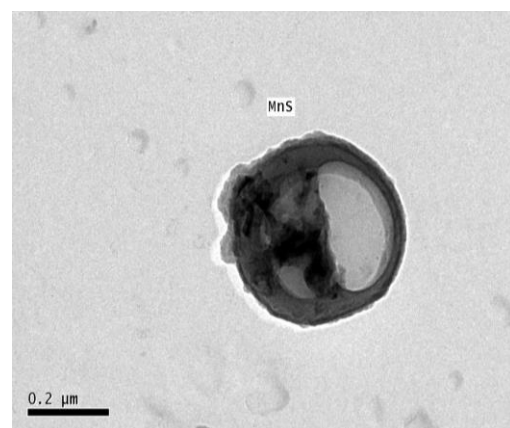


Fig. 2. Morphology of the second particles

Controlling precipitation behavior of second phase particles is important for obtaining proper microstructures and excellent magnetic properties of electrical steels. The dispersed particles are often formed during hot rolling. Dislocations produced by hot deformation offer nucleation

sites of second phase particles and favor dispersive precipitation. On the other hand, the possible recovery and recrystallization in the deformed matrix under high temperature condition would reduce the dislocation density, which is unfavorable for dispersive precipitations. In general, industrial deformation process with decreasing temperature during all the process plays an important role for the precipitation behavior controlled by thermal activation.

3.2 Texture inheritance

The texture of the test steel coils A and B after same treatments was studied with the aid of ODFs. It is known that the most frequently encountered orientations in the texture of deformation and recrystallization of bcc metals are present in the ODF section at $\phi_2=45^\circ$ (see Fig. 3). Among these characteristic orientations, it is possible to distinguish a limited axial component $\langle 111 \rangle$, in which the normal to the grain planes $\{111\}$ are parallel to the direction of the normal to the rolling plane (ND), and a limited axial component $\langle 110 \rangle$, in which the corresponding directions in the grains are parallel to rolling direction (RD) in the sheet. These components are sometimes referred to as the axial components γ and α respectively. It is natural that useful orientations in the sheet of isotropic steel after a finishing treatment would be orientations with the planes $\{100\}$ parallel to the rolling plane (the upper side of the square of the section of the space of the Euler angles, the axial component η) and with the planes $\{110\}$ parallel to the rolling plane (the lower side of the square of the section of the space of the Euler angles), since in the grains with such orientations the most frequently encountered easy axis is $\langle 100 \rangle$. The planar orientation $\{111\}$ typical of their crystallization texture of the iron-silicon alloy will be most unfavorable.

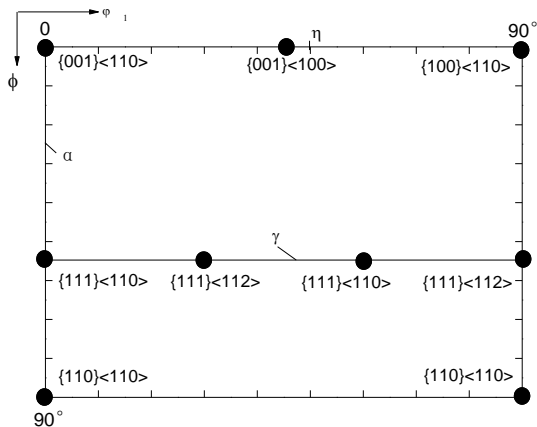
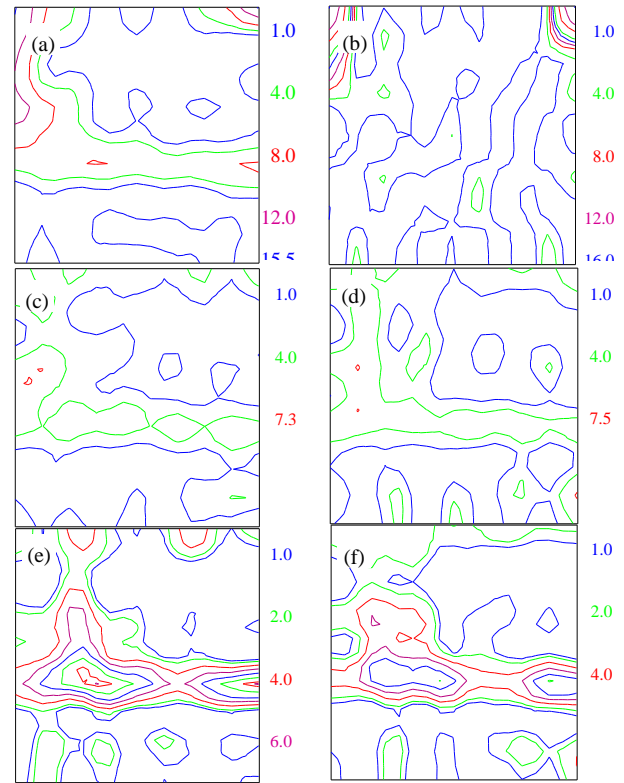


Fig. 3. Positions of ideal orientations in the section of the space of Euler angles at $\phi_2=45^\circ$



(a), (b) hot-brand; (c), (d)normalization coil; (e)(f) annealing coil
Fig. 4. Sections of ODF at $\phi_2=45^\circ$

Fig. 4 displays the textures of hot rolling, normalization and annealing of the test steels A and B. After hot rolling process the steel A has a sufficiently sharp texture (see Fig.4a) with typical limited axial orientations γ and α . In the case of the axial component γ , the greater density is characteristic of the $\{001\} \langle 110 \rangle$ and $\{112\} \langle 110 \rangle$ orientations, but the texture of the steel B becomes more diffuse (see Fig.4b). The greater density is characteristic of the $\{001\} \langle 110 \rangle$ orientations.

After normalization process the steel A and B have structural similitude texture (see Fig. 4c&d). But the steel B density is lower in $\{112\} \langle 110 \rangle$ and $\{111\} \langle 110 \rangle$ orientations than that of in steel A. Goss texture becomes stronger in steel A and steel B especially in steel B.

After annealing process the steel A and B have structural similitude texture still (see Fig. 4e&f). The $\{111\}$ orientation becomes strongest. But the steel B density is lower in $\{111\}$ orientations than that of in steel A.

Fig. 5 shows the intensity of different deformed textures. The deformed texture is inhomogeneous along the RD-fiber (α -fiber). The peak value emerges at $\{001\} \langle 110 \rangle$ orientation. The steel coil B surface texture $\{001\} \langle 110 \rangle$ component is the strongest. However, the deformed texture is homogeneous along the ND-fiber (γ -fiber); the intensity of $\{111\} \langle 112 \rangle$ component is the strongest and that of $\{111\} \langle 110 \rangle$ is the second strongest. Steel coil A's $\{100\}$ surface textures to be less than the steel coil B's $\{100\}$ surface textures, and the steel coil A $\{111\}$ surface

textures than B {111} surface texture.

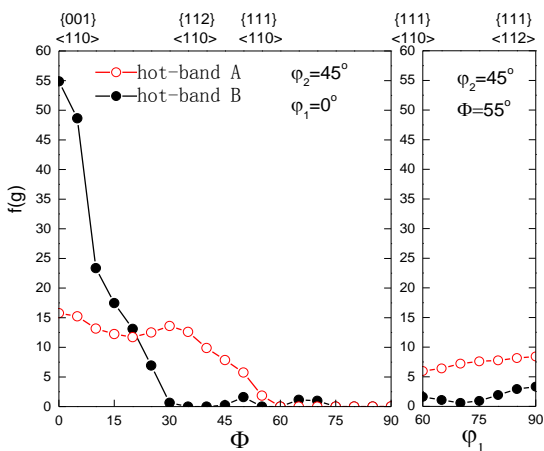


Fig. 5. Orientation distribution intensities of hot-band specimens

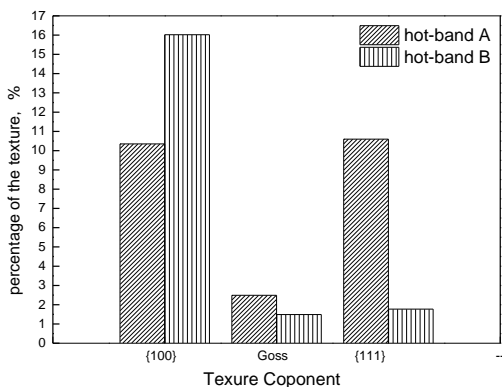


Fig. 6. Percentage of the hot-band texture

The percentage of the hot-band texture is represented in Fig. 6, in which the steel coil A's surface texture {100} accounted for 10.35%, Goss 2.49%, {111} texture 10.6%; steel coil B's surface texture {100} accounted for 16.02%, Goss 1.49%, {111} texture 1.77%. In the hot-band specimen, the percentage of the surface texture {100} and {111} components is much larger, whereas that of Goss is smaller. The steel coil A's surface texture {111} is much larger than the steel coil B surface texture {111}.

Fig. 7 shows the intensity of different normalization textures. The normalization texture is homogeneous along the RD-fiber (α -fiber). Steel coil A's {100} surface textures to be less than the steel coil B's {100} surface textures, and the steel coil A's {111} surface textures than B's {111} surface texture.

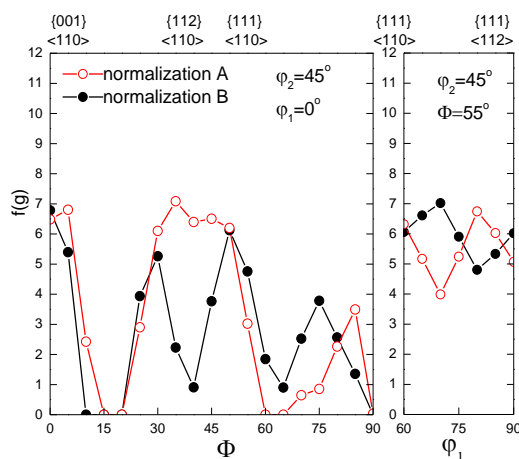


Fig. 7. Orientation distribution intensities of normalization specimens

The percentage of the normalization texture is represented in Fig. 8, in which the steel roll A's surface texture {100} accounted for 7.91%, Goss 4.94%, {111} texture 7.06%; steel coil B's surface texture {100} accounted for 5.22%, Goss 9.65%, {111} texture 5.16%. In the normalization specimen, the percentage of the Goss components is much larger, whereas that of surface texture {100} is smaller. The steel coil B's Goss texture is much larger than the steel coil A's Goss texture.

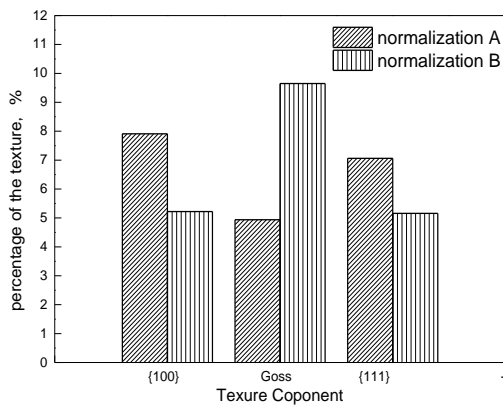


Fig. 8. Percent of the normalization texture

Fig. 9 shows the intensity of different annealing textures. The annealing texture is homogeneous along the RD-fiber (α -fiber). The peak value emerges in {111} <110> orientation. However, the annealing texture is inhomogeneous along the ND-fiber (γ -fiber); the intensity of {111} <112> component is strong in steel A. The steel coil A's {100} and {111} surface texture is less than the steel coil B {100} surface texture.

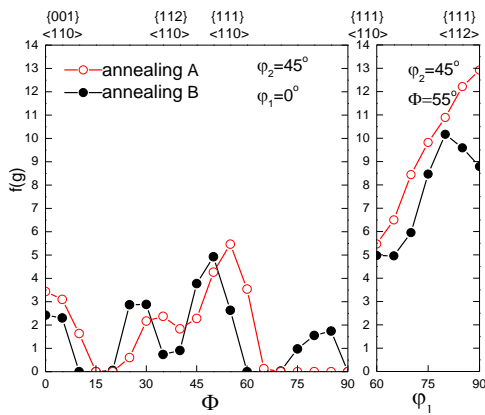


Fig. 9. Orientation distribution intensities of annealing specimens

The percentage of the annealing texture is represented in Fig. 10, in which the steel coil A's surface texture {100} accounted for 5.84%, Goss 1.91%, {111} texture 13.05%; steel coil B's surface texture {100} accounted for 5.73%, Goss 2.83%, {111} texture 10.45%. In the annealing specimen, the percentage of all the surface texture changed lower. The percentage of steel coil B's Goss is higher than that the steel coil A.

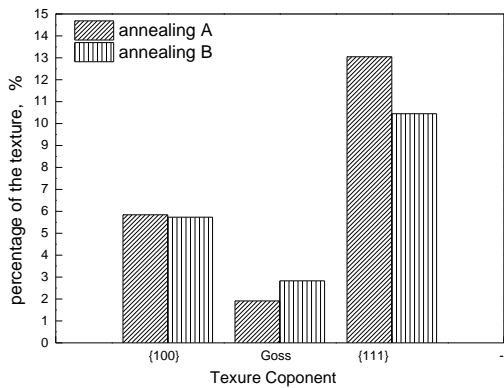


Fig. 10. Percent of the annealing texture

Fig. 11 shows the value of the proportion of the texture for $[\{100\} + \text{Goss}] / \{111\}$. The steel coil A's value of $[\{100\} + \text{Goss}] / \{111\}$ is 1.212 in hot-band, 1.82 in normalization coil and 0.59 in annealing coil; The steel coil B's value of $[\{100\} + \text{Goss}] / \{111\}$ is 9.89 in hot-band, 2.88 in normalization coil and 0.82 in annealing coil.

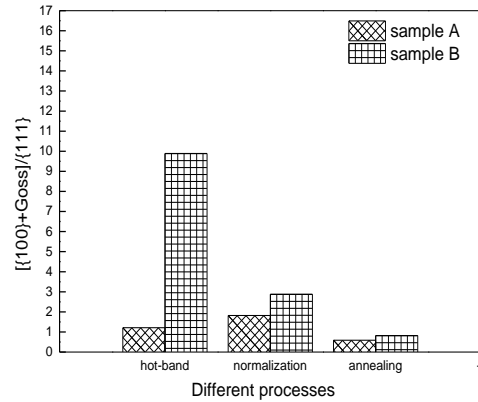


Fig. 11. $[\{100\} + \text{Goss}] / \{111\}$ of the different process

Fig. 12 shows steel coil A's annealed iron loss is 2.68W/kg and magnetic induction was 1.673T; steel coil B's annealed iron loss is 2.61W/kg, magnetic induction 1.681T.

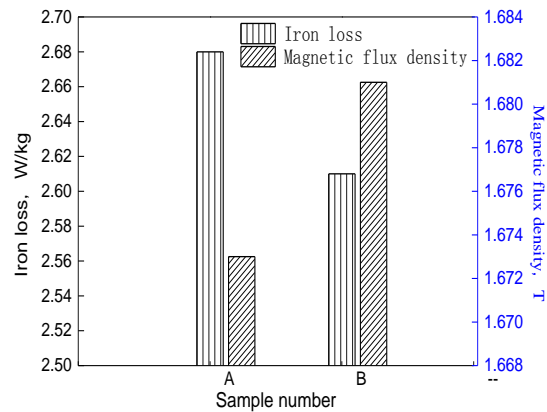


Fig. 12. Magnetic properties after annealing process

Observed in Fig. 11, we noticed that the proportion of the texture for $[\{100\} + \text{Goss}] / \{111\}$ in the steel coil B is always higher than that of in the test steel A in the hot, normalizing and annealing process. Fig. 12 shows iron loss value of the steel coil B is lower than that of the steel coil A. and magnetic flux density of the steel coil B is higher than that of the steel coil A. The worse of the value of the proportion of the rolling texture for $[\{100\} + \text{Goss}] / \{111\}$ is the worse that of the annealing. The better of the value of the proportion of the texture for $[\{100\} + \text{Goss}] / \{111\}$ is the better magnetic properties. All these fully reflect the texture hereditary. Gauss texture promotes magnetic induction increases.

4. Conclusion

1) MnS promotes particle nucleation during hot rolling and retards recrystallization in the normalization and annealing process.

2) The characteristic of initial organization decided to organizational characteristics of the following the process, which reflects the organization of hereditary

3) The bigger of the value of the proportion of the texture for $\{100\} + \text{Goss} / \{111\}$ is better magnetic properties, which reflect the texture hereditary.

4) Gauss texture promotes magnetic induction increases.

5) Through hereditary studies, we can control the organization to control the texture pattern, control magnetic properties finally.

Acknowledgments

We would like to thank the National Natural Science Foundation of China (51374132) and Science and technology research Foundation of Science and Technology Department of Henan Province of China (No.132102210481) for financial support.

References

- [1] Z. Z. He, *Electrical Steel*. Beijing: Chinese Metallurgy Engineering Press, Beijing (1996).
- [2] S. C. Paolinelli, M. A. da Cunha da, *Journal of Magnetism and Magnetic Materials*. **304**, e596 (2006).
- [3] Y. Sidor, F. Kovac, *Materials Characterization* **55**, 1 (2005).
- [4] A. Chaudhury, R. Khatirkar, N. N. Viswanathan, V. Singal, A. Ingle, S. Joshi, I. Samajdar, *Journal of Magnetism and Magnetic Materials*. **313**, 21 (2007).
- [5] L. A. Prisekina, L. B. Kazadzhan, Y. I. Larin, I. N. Krutskikh, *Metallurgist*. **32**, 154 (1988).
- [6] C. M. B. Bacaltchuk, G. A. Castello, M. Ebrahimi, *Scripta Materialia*. **48**, 1343 (2003).
- [7] J. T. Park, J. A. Szpunar, *Journal of Magnetism and Magnetic Materials*, **321**, 1928 (2009).
- [8] T. Ye, C. Zhou, Z. Y. Gao, *Journal of Functional Materials*, **45**, 03110 (2014).
- [9] H. Dong, Y. Zhao, X. J. Yu, F. Z. Lian, *Journal of Iron and Steel Research*. **6**, 86 (2009).
- [10] S. S. F. de Dafe, S. C. Paolinelli, A. B. Cota, *Journal of Magnetism and Magnetic Materials*, **323**, 3234 (2011).
- [11] Y. Zhang, Y. Xu, B. Xu, H. Liu, G. Chao, Z. Y. Liu, G. D. Wang, *Journal of Magnetism and Magnetic Materials*, **324**, 3328 (2012).
- [12] J. Barros, J. Schneider, K. Verbeken, Y. Houbaert, *Journal of Magnetism and Magnetic Materials*, **320**, 2490 (2008).
- [13] D. N. Lee, H. S. Choi, H. N. Han, *Metals and Materials International*. **17**, 879 (2011).
- [14] D. S. Petrovic, B. Markoli, M. Ceh, *Journal of Magnetism and Magnetic Materials*, **322**, 3041 (2010).
- [15] W. Mao, Z. An, W. Guo, P. Yang, *Steel research international*, **81**, 477 (2010).
- [16] K. Jenkins, M. Lindenmo, *Journal of Magnetism and Magnetic Materials*, **320**, 2423 (2008).
- [17] L. Xiang, E. B. Yue, D. D. Fan, St. Qiu P. Zhao, *Journal of Iron and Steel Research, International*, **15**, 88 (2008).

*Corresponding author: yetie2009@sina.com